Phase stability control of interstitial oxide ion conductivity in the $La_{1+x}Sr_{1-x}Ga_3O_{7+x/2}$ melilite family

Chris I. Thomas, *Xiaojun Kuang*, *Zengqiang Deng*, *Hongjun Niu*, *John B. Claridge* and *Matthew J. Rosseinsky**

Department of Chemistry

University of Liverpool, Liverpool, L69 7ZD, UK

Received:

Corresponding author. E-mail: rossein@liverpool.ac.uk.

Abstract

The two-dimensional polyhedral anion network melilites $La_{1+x}Sr_{1-x}Ga_3O_{7+0.5x}$ exhibit interstitial oxide ion conductivity. The solid solution is shown to extend to x = 0.64 and the variation of the conductivity with x is investigated. At high temperatures all of these compounds adopt the typical tetragonal melilite structure. When x > 0.6, cooling below 600 °C results in a reversible phase transition to an orthorhombic structure which reduces the ionic conductivity. Quenching experiments have shown the tetragonal structure has a higher conductivity compared to the orthorhombic structure of the same composition. Short-range order effects associated with this transition exercise an important influence on the composition- and temperature-dependence of the conductivity.

Keywords: Ceramics, Fuel Cells, Oxide Ion Conduction and Structure-Property Relationships

Introduction

Solid Oxide Fuel Cells (SOFCs) have particular advantages over other types of fuel cell such as modularity and fuel flexibility[1] with the ability to use a range of fuels from high purity H_2 to readily available hydrocarbons.[2] However current SOFCs require high temperatures e.g. above 700 °C for Yttria stabilized zirconia (YSZ)[3] or above 500 °C for gadolinium doped cerium oxide (CGO)[4] systems for operation. At these temperatures the ions become mobile enough for efficient operation of the cell but the thermal expansion and reactivity of the fuel cell components becomes problematic[5]. For SOFCs to become competitive with current technology, oxide ion electrolytes with specific conductivities exceeding 10^{-2} Scm^{-1} at low (~ 500 °C) temperatures are required,[6] motivating the search for materials displaying new combinations of carrier and structure type.

Recently the two-dimensional complex anion network melilites[7, 8] $La_{1+x}Sr_{1-x}Ga_3O_{7+0.5x}$ have been shown to exhibit interstitial[9] oxide ion conduction of 0.02-0.1 S/cm at x = 0.54 over the 600-900 °C temperature range – this is unusual, as interstitials are usually found in isolated anion rather than network structures. Rozumek and co workers present data from x = -0.15 to x = 0.60 while Kuang and coworkers[9] suggest that x = 0.6 is the maximum value of x which will retain the parent structure with disordered oxide ion interstitials. The x = 0 parent material $LaSrGa_3O_7$ is tetragonal (T) (a_{tetra} =8.056 Å, c_{tetra}=5.333 Å [10] (Figure 1)). La and Sr occupy the eight coordinate A site while the smaller Ga occupies two distinct tetrahedral sites (3-connected, with a non-bridging terminal oxide, and 4-connected with all oxides bridging to neighboring tetrahedra) in a corner-shared tetrahedral 2D layer with a distorted pentagonal tunnel which is occupied by the interstitial oxygen charge carriers required for charge balance when x > 0. Above and below the center of each tunnel are the A sites (Figure 1). This paper addresses the limits on the extent of La substitution for Sr in single-phase materials and thus on the interstitial anion carrier density and ionic conductivity. The highest carrier concentrations produce long-range static structural ordering of the interstitials which strongly influences the ionic transport.

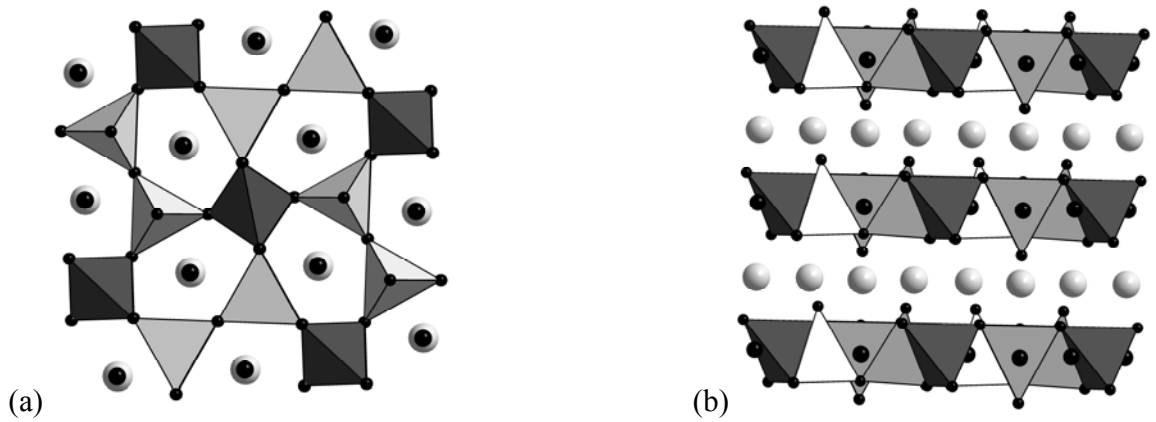

Figure 1. The melilite structure of $LaSrGa_3O_7$ showing the two types of GaO_4 tetrahedra (dark grey 4-connected, light grey/white 3-connected). Light grey spheres show the La/Sr sites and the black spheres show oxygen. The spheres for the interstitial oxygen sites are larger than those for the framework oxygens. In (a) the view is down the c axis showing the Ga tetrahedra and the pentagonal tunnels. The view in (b) along [110] shows that the interstitial oxygen sits in the center of the Ga layers with La/Sr cations above and below.

Experimental:

Synthesis and processing: Phase relations of La_2O_3-SrO-Ga_2O_3 in the $La_{1+x}Sr_{1-x}Ga_3O_{7+0.5x}$ series were investigated by solid state reaction using La_2O_3 (99.999%, Alfa Aesar), $SrCO_3$ (99.995%, Aldrich) and Ga_2O_3 (99.999%, Alfa Aesar) as starting materials, which were mixed in ethanol and calcined at 1200 °C for 12 h. Due to La_2O_3 absorbing water and CO_2 at ambient temperatures the La_2O_3 powder was stored in a furnace at 950 °C prior to weighing. After regrinding, the powders were uniaxially pressed into pellets, placed on platinum foil (99.95%, Goodfellow Ltd), in covered alumina crucibles (Almath Crucibles Ltd 99.8 %) and fired at 1400 °C (x = 0-0.54) or 1350 °C (x = 0.56-0.64) for 12 h. To counter the volatilization of Ga at high temperatures a small excess was required meaning that instead of the 2:3 La/Sr:Ga ratio, this was 2:3.05 (1.7% excess Ga) for x = 0.54 - 0.58 2:3.06 (2% excess Ga) for x = 0.6 and x = 0.62, and 2:3.07 (2.3% excess Ga) for x = 0.64. Post synthesis XRD showed no evidence of Ga_2O_3 or other gallium rich impurities being present. If stoichiometric quantities or higher

temperatures than stated above are used a melilite phase is observed as the main phase but a perovskite phase is also visible in the powder XRD data.

Pellet samples with > 90% of the theoretical density for electrical measurements were made via cold-isostatic pressing (CIP) with 206.85 MPa pressure after being calcined at 1200 °C for 12 h, followed by the final firing at 1350 °C for 12 h.

Quenching experiments were carried out by removing the alumina crucible from the furnace at 1350 °C and tipping the pellet out onto a block of aluminium at room temperature.

Characterization: The phase purity was checked by powder X-ray diffraction data with a Panalytical X'pert Pro Multi-Purpose X-ray diffractometer (Co $K\alpha_1$ radiation λ = 1.78901Å) collected at ambient temperature. Silicon was added as an internal standard to refine the cell variation with composition. For the time resolved study a sample of metastable quenched T structured $La_{1.64}Sr_{0.36}Ga_3O_{7.32}$ in a 0.5 mm outside diameter amorphous fused silica capillary (Mark-Röhrchen quarzkapillaren) was measured at station I11 of the Diamond Light Source. Data were collected step-wise over 1.821-141.953 2θ (λ = 0.82545 Å) in sequential five minute datasets collected at 400 °C. Using the same wavelength, a separate capillary was heated from 300 °C to 600 °C. Five minute datasets were collected over the same 2θ range in 5 °C steps with a ramp rate of 5 °C per minute between scans. At 600 °C a 20 minute scan was taken of the sample at the end of the heating protocol.

Conductivity Measurement: Ac Impedance Spectroscopy (IS) measurements in air were performed with a Solartron 1255B Frequency Response Analyzer coupled to a Solartron 1287 electrochemical interface over the 10^{-2}-10^{6} Hz frequency range for measurements in the 350-980 °C range.

Pellets were prepared by first polishing both sides with Silicon Carbide paper, (Buehler P800 and P2500) then applying the electrodes. The electrodes used were made by painting the polished pellet with platinum paste (Metalor A4731) and firing at 150 °C for 1 hour, then ramping to 300 °C holding for 1 hour then ramping to 800 °C holding for 1 hour then ramping to 950 °C for the measurement. The ramp

rate was set at 5 °C per minute and the wires used to connect the pellet to the Solartron leads were Engelhard CPPT platinum wire.

For each sample the pellet being measured was heated to 950 °C and left to dwell for an hour before the measurement took place. Measurements were then taken every 50 °C down to 350 °C with the measurement for each temperature only occurring after the sample had been left for 1 hour at that temperature to ensure the sample had equilibrated.

The bulk and the grain boundary responses at higher frequencies overlap to exhibit part of an asymmetric semicircular arc. The intercept of the semicircular arc at low frequency was extracted as the total resistivity $R_b + R_{gb}$. Above 400 °C, the electrode response dominated the impedance data and gradually collapsed to a semicircular arc, giving two arcs in the impedance plot. The high frequency intercept of the second arc was taken as total resistivity $R_b + R_{gb}$ while the high frequency intercept of the first arc was taken as the bulk resistivity R_b. This allows the bulk and grain boundary resitivities to be separated over the region where the two arcs are visible (Figure S4). As the temperature is increased the arc from the grain boundary response vanishes and only one semicircular arc from the electrode response was seen with the high frequency intercept being taken as the total resistivity $R_b + R_{gb}$.

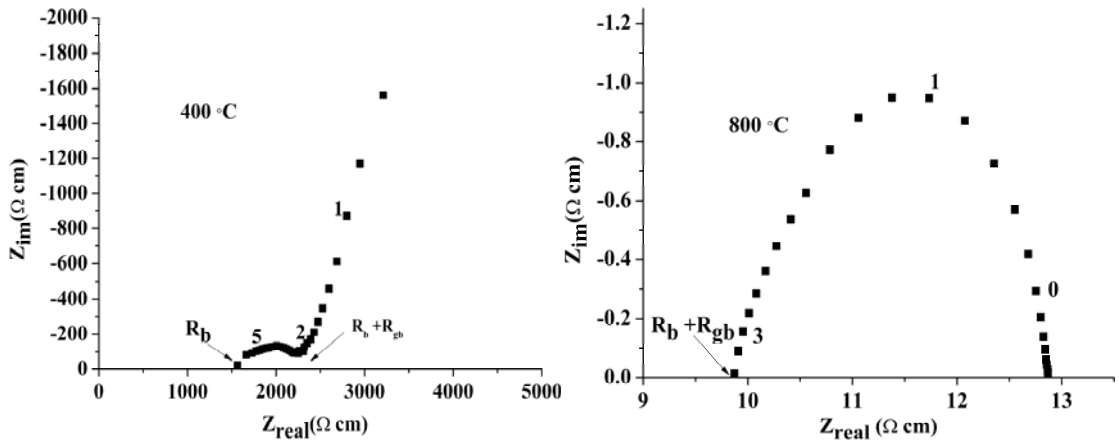

a) b)

Figure 2 Complex impedance plots of $La_{1.6}Sr_{0.4}Ga_3O_{7.3}$ at 400 ˚C (a) and 800 ˚C (b). The numbers in bold on the plot indicate the frequency logarithms, the a.c. amplitude used for the measurements was 10 mV.

Measurement of the conductivity of a quenched T sample of $La_{1.64}Sr_{0.36}Ga_3O_{7.32}$ on heating from 200 °C to 500 °C and subsequent cooling to 200 °C was performed to compare the conduction behaviors of tetragonal (T) and pseudo-orthorhombic phase (O) on materials with same composition. The measurement was taken in 25 °C intervals over the entire temperature range with one hour equilibration time at each temperature. For the quenched samples of $La_{1.64}Sr_{0.36}Ga_3O_{7.32}$ a Solartron 1296 dielectric interface was used instead of the Solartron 1287 electrochemical interface for measurements over the 10^{-2}-10^{6} Hz frequency range and the temperature range 200 °C – 500 °C on heating and cooling cycles. Instead of platinum electrodes, silver conductive paint which dries in air was used (Agar G3790) to allow for measurement to be carried out without the need to sinter electrodes at high temperatures. Note that at each temperature the samples dwell for 1 hour, so the points for both cooling post 500 °C and for the furnace cooled sample will be single phase O. Further measurement on one more heating and cooling cycle from 200 °C to 500 °C after the conversion from the T phase to the O phase described in the text did not show significant change in the conductivity, suggesting the O phase is stable to thermal cycling.

The a.c. conductivity as a function of partial pressure of oxygen (pO_2) (monitored by a YSZ potentiometric sensor) was measured at 600 °C over a pO_2 range of 1-10^{-22} atm. The pO_2 value was controlled over 1-10^{-4} atm pO_2 range by dilution of O_2 with Ar, for 10^{-4}-10^{-22} atm by using mixed 1%CO in Ar and 1% CO_2 in Ar. The dwell time ranged from 5 – 24 h (~5-8 h for $pO_2 > 10^{-4}$ and 12-24 h for $pO_2 < 10^{-4}$ to allow equilibration of the samples with the gas environment at each point.

Diffuse Reflectance: The band gap of $LaSrGa_3O_7$ was measured on a polycrystalline sample using diffuse reflectance spectroscopy. Reflectance data were collected on a Perkin Elmer LAMDA 650 S UV/Vis spectrometer using $BaSO_4$ reflectance standards and converted to absorbance (using Kubelka-Munk). The band gap energy was then obtained by using the Shapiro method of extrapolating the onset of absorption to the wavelength axis.[25]

Infrared spectroscopy (IR): The IR measurement was carried out on a Perkin Elmer Spectrum 100 with ATR.

Thermo gravimetric analysis (TGA): The TGA measurement was carried out using a TA Instruments SDTQ600

Energy-dispersive X-ray analysis (EDS): The EDS was carried out using a JEOL 2000FX transmission electron microscope operated at 200 kV.

Results

Ceramic synthesis with slight (< 3% depending on x, see experimental details) excess Ga_2O_3 affords the $La_{1+x}Sr_{1-x}Ga_3O_{7+0.5x}$ ($x \leq 0.64$) samples studied here (x = 0.65 and x = 0.67 were also studied but did not afford single phases, instead forming a mixture of melilite and Sr-doped $LaGaO_3$ (LSG). The powder X-Ray (XRPD) patterns (Figure 3**)** for x < 0.6 can be indexed using the T cell of the parent phase. However, for x > 0.6, the splitting of the $h,k \neq 0$ tetragonal reflections requires indexing with a pseudo-orthorhombic (O) cell ($a_{orth} \approx b_{orth} \sim \sqrt{2}a_{tetra}$, $c = c_{tetra}$).

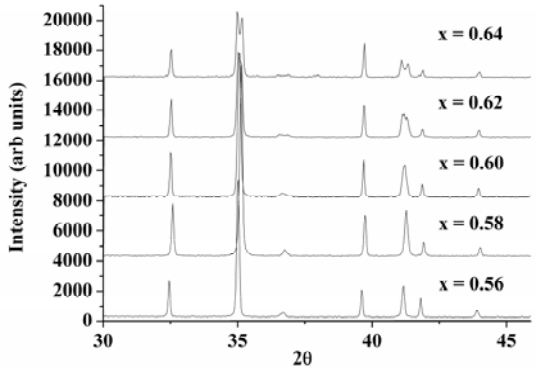

Figure 3. XRD patterns of $La_{1+x}Sr_{1-x}Ga_3O_{7+x/2}$ (x = 0.56. 0.58, 0.6, 0.62 and 0.64).

The true symmetry may be lower. The *a* parameter (Figure 4 (a)) decreases linearly with x until the transition to the O structure, with the *c* parameter and the volume (Figure 4 (b)) decreasing linearly across the entire composition range, accounted for by the smaller size of La^{3+}. x = 0.64 is the highest La content affording a single phase composition and is O at room temperature.

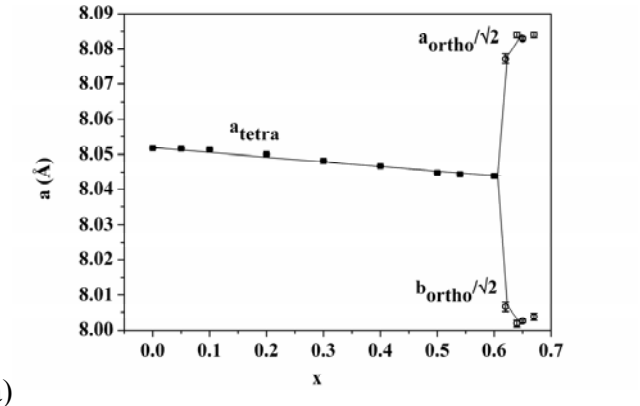

(a)

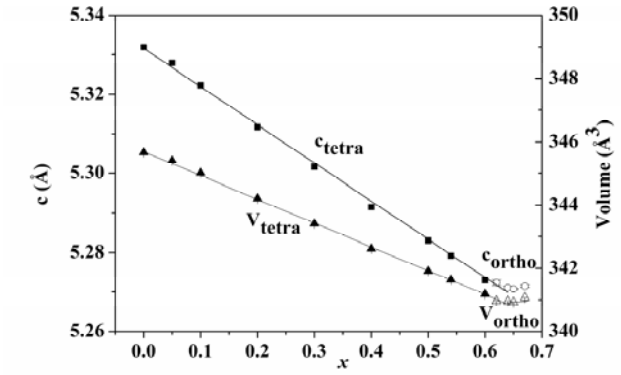

(b)

Figure 4. (a) *a* and *b* lattice parameters (b) *c* parameter and unit cell volume of $La_{1+x}Sr_{1-x}Ga_3O_{7+x/2}$, x = 0 to x = 0.67. Data for x < 0.6 are from 9 , for x > 0.6 this work.

Variable temperature powder X-ray diffraction data for $La_{1.64}Sr_{0.36}Ga_3O_{7.32}$ (Figure S3) shows the O to T transition takes place at 565 ^oC on heating. This transition can also be observed in the conductivity data as a change in the gradient (activation energy) of a ln(σT) versus 1/T plot (Figure 8). An in-situ PXRD scan at 600 °C was fitted using the LeBail method shown in Figure 5 (a) showing that at 600 °C the pure T phase was observed. The transition from T to O is controlled by kinetic factors, demonstrated by furnace-cooled samples with x > 0.6 showing the presence of both phases (Figure 5 (b)).

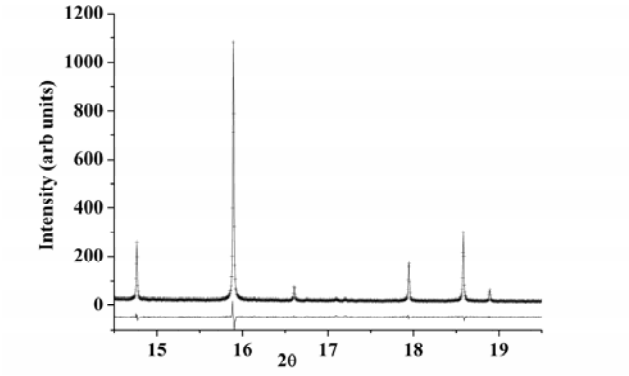

(a)

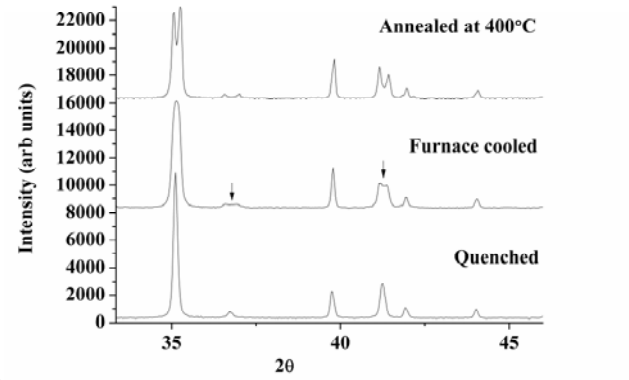

(b)

Figure 5. (a) LeBail fit of $La_{1.64}Sr_{0.36}Ga_3O_{7.32}$ at 600 ˚C using the tetragonal space group $P\bar{4}2_1m$ (λ= 0.825451Å, R_{wp} =7.965%) (b) $La_{1.64}Sr_{0.36}Ga_3O_{7.32}$ after quenching, furnace cooling and annealing for 12 hours at 40O ˚C. The arrows indicate the tetragonal peaks in the pseudo-orthorhombic dominated furnace-cooled sample.

Pure T $La_{1.64}Sr_{0.36}Ga_3O_{7.32}$ can be prepared by quenching to room temperature from the high temperature T phase stability region at 1350 °C, with the mixed O and T phases accessed by furnace cooling at 15 °C min^{-1} . The pure O phase is produced by annealing either quenched T or furnace cooled T/O samples for 12 hours at 400 °C. In-situ PXRD data at 400 °C revealed that the $h,k \neq 0$ single reflections of the quenched metastable T phase broadened and split completely within 30 minutes to obtain the single phase stable O structure (Figure 6 (a)).

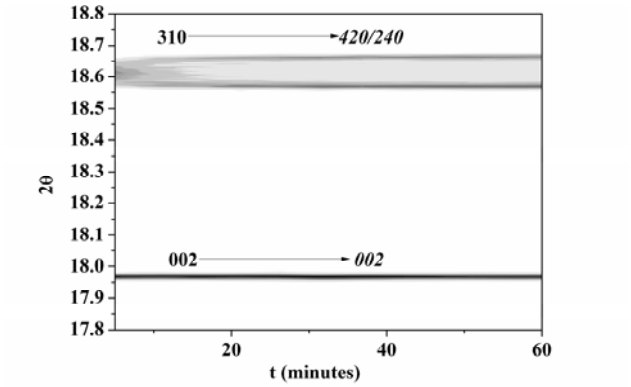

(a)

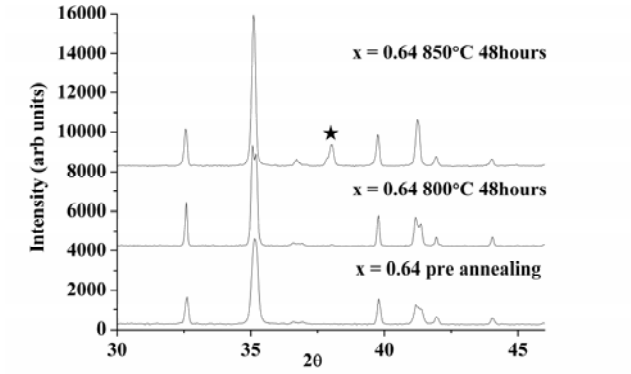

(b)

Figure 6. (a) Diffraction from $La_{1.64}Sr_{0.36}Ga_3O_{7.32}$ at 400 ˚C showing the transition from metastable T to stable O phase. T Miller indices in bold and O in italics. (b) XRD patterns of $La_{1.64}Sr_{0.36}Ga_3O_{7.32}$ before annealing, after annealing at 800 ˚C for 48 hours and after 850 ˚C for 48 hours. Black star shows the formation of strontium doped lanthanum gallate (LSG) perovskite.

The synthesized samples are stable to 800 ºC in air (Figure 6 (b)). For $x \geq 0.4$, prolonged annealing above this temperature (for periods longer than the impedance measurements described later – all materials reported were examined by XRD post-measurement to ensure their single phase nature was retained) causes the melilite to partially decompose with formation of the Sr-doped LSG perovskite (Figure (6b), black star) and Ga_2O_3 as detailed in SI (Figures S9, S10), rendering conductivity comparisons with $La_{0.8}Sr_{0.2}Ga_{0.83}Mg_{0.17}O_{2.815}$ (LSGM) only meaningful below 800 °C at these higher

doping levels. The instability with respect to LSG only occurs over a limited temperature range – reheating the phase separated mixture at 1350 °C affords the initial melilite, suggesting a complex sequence of phase stability (Figure S11).

Impedance data from the $La_{1+x}Sr_{1-x}Ga_3O_{7+0.5x}$ materials (Figures 2a & 2b) at < 400 °C exhibit a significant Warburg electrode[11, 12] response with an associated large capacitance (>10^{-7} F cm^{-1}) in the low frequency range (<10 Hz), which is characteristic of ionic conduction with partially blocking electrodes. The total conductivity of $La_{1.64}Sr_{0.36}Ga_3O_{7.32}$ at 600 °C is independent of oxygen partial pressure over the 1-10^{-22} atm range (Figure 7), as found earlier for $La_{1.54}Sr_{0.46}Ga_3O_{7.27}$ [9] showing that there is pure ionic conductivity across the entire series $La_{1+x}Sr_{1-x}Ga_3O_{7+x/2}$ to the solid solution limit x = 0.64. Post measurement XRD of $La_{1.64}Sr_{0.36}Ga_3O_{7.32}$ (Figure S12) shows that the sample remains single phase.

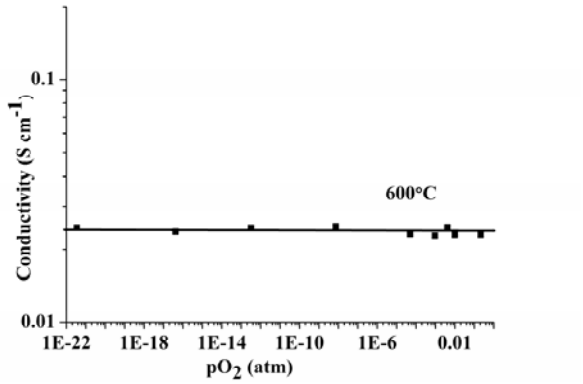

Figure 7. pO_2 dependence of the total conductivity of $La_{1.64}Sr_{0.36}Ga_3O_{7.32}$ at 600 ºC.

The band gap of $LaSrGa_3O_7$ (measured by diffuse reflectance Figure S7) is 5.0 eV, consistent with the absence of an intrinsic electronic contribution over the entire temperature range measured.

The transition at 565 °C to the O structure on cooling in $La_{1.64}Sr_{0.36}Ga_3O_{7.32}$ produces a sharp reduction in the conductivity (Figure. 8) associated with an increase in activation energy from 0.57 eV to 1.2 eV, and is thus assigned to the long-range ordering of the oxygen interstitial charge carriers.

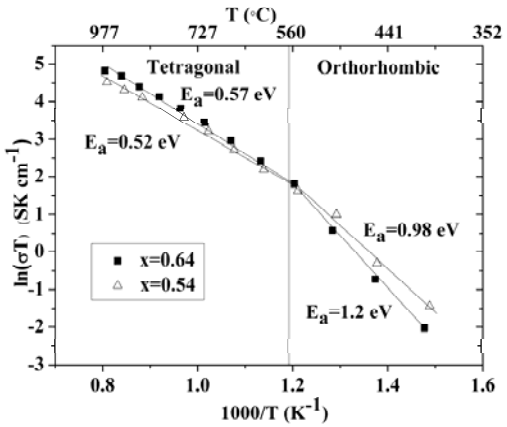

Figure 8. Conductivity of $La_{1.64}Sr_{0.36}Ga_3O_{7.32}$ (black squares, T at high temperature, O at low temperature) and $La_{1.54}Sr_{0.46}Ga_3O_{7.27}$ (triangles, T at all temperatures). The lines show the two regions with different activation energies. The post-measurement XRD is given in Figure S5a.

The total conductivity (Figure 9) of a quenched $La_{1.64}Sr_{0.36}Ga_3O_{7.32}$ T phase pellet on heating over the 200-300 °C temperature range is approximately two orders of magnitude higher than that on cooling through this range after heating to 500 °C to form the ordered O phase (e.g. 1.55 x 10^{-4} Scm^{-1} on heating (T) against 5.5 x 10^{-6} Scm^{-1} cooling (O) at 300 °C), consistent with the T phase corresponding to disordered and the O phase to ordered carriers. The activation energy (0.95eV) for the quenched metastable T $La_{1.64}Sr_{0.36}Ga_3O_{7.32}$ over 200-300 °C measured on heating (Figure 9), compares to 0.85eV for tetragonal $La_{1.54}Sr_{0.46}Ga_3O_{7.27}$ at low temperature (250 °C – 400 °C) reported by Kuang and to 0.98 eV for the stable O phase in this temperature range. With increasing temperature the conductivity of the virgin quenched T phase pellet remains higher than the furnace cooled mixed phase sample until approximately 400 °C, where the conductivity matches that of the furnace cooled sample. This is consistent with formation of the O phase in quenched samples (Figure 6 (a)) within 30 minutes at this temperature. The conductivity on cooling post 500 °C measurement completely matched that for the furnace-cooled $La_{1.64}Sr_{0.36}Ga_3O_{7.32}$ pellet.

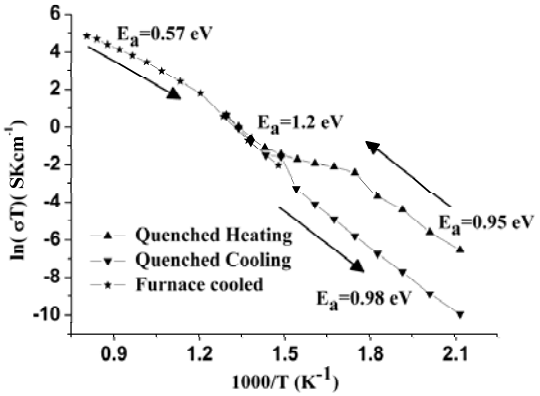

Figure 9. The conductivity of quenched $La_{1.64}Sr_{0.36}Ga_3O_{7.32}$ during thermal cycling is given by triangles. Initially the sample is tetragonal converting to orthorhombic on heating above 400 ºC, on cooling this sample retains the orthorhombic structure. The conductivity of a second sample of $La_{1.64}Sr_{0.36}Ga_3O_{7.32}$ which was furnace cooled from 1350 ºC is also given for comparison and denoted by stars. This material adopts the tetragonal structure above 565 ºC below, which it reverts to the orthorhombic structure. Post-measurement XRD of the furnace cooled sample (stars) is shown in Figure S5a post measurement XRD of the quenched sample (triangles) is shown in Figure S5b.

Discussion

The total conductivity versus temperature in air for $0 \leq x \leq 0.64$ is shown in Figure 10 (a) with $La_{0.8}Sr_{0.2}Ga_{0.83}Mg_{0.17}O_{2.815}$ [13] (LSGM) for comparison. The conductivity at x = 0.54 is approximately three orders of magnitude greater than the parent material. The total conductivity of x = 0.6 $La_{1.6}Sr_{0.4}Ga_3O_{7.3}$ at 500 °C is 6.8 x 10^{-3} Scm^{-1}, which compares with 4 x10^{-3} Scm^{-1} for the bulk conductivity of Mg-doped $La_{10}Si_6O_{27}$, [14] 3.2 x 10^{-4} Scm^{-1} for the bulk conductivity of Al-doped $La_{10}Ge_6O_{27}$, [15] 5 x 10^{-3} Scm^{-1} for the total conductivity of LSGM ($La_{0.8}Sr_{0.2}Ga_{0.83}Mg_{0.17}O_{2.815}$) [13] and 0.004-0.01 Scm^{-1} for the total conductivity of $Ce_{0.9}Gd_{0.1}O_{1.95}$.[4, 17, 18] Above 600 °C and below 400 °C, all the interstitial-based melilites are poorer conductors than vacancy-based LSGM, but over the 400-

600 °C range, the x = 0.58 and x = 0.6 compositions have slightly higher conductivity than LSGM (Figure 10 (a)).

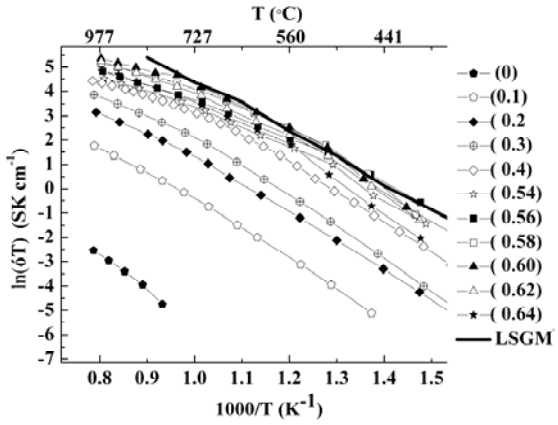

(a)

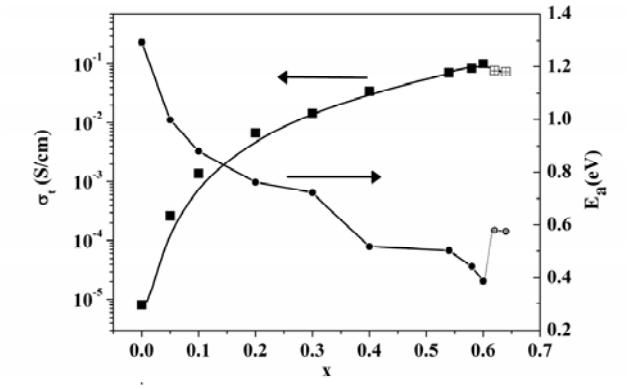

(b)

Figure 10. (a) Conductivity of $La_{1+x}Sr_{1-x}Ga_3O_{7+x/2}$ where x = 0 - 0.64; LSGM is $La_{0.8}Sr_{0.2}Ga_{0.83}Mg_{0.17}O_{2.815}$.[13] In Figure 10 (a) x = 0.64 and the furnace cooled data in Figure 9 are the same measurement. (b) Conductivity and activation energy of $La_{1+x}Sr_{1-x}Ga_3O_{7+x/2}$ at 800 ºC versus x. The low temperature stable forms are indicated by filled (T) and empty (O) symbols. The black curved line for the conductivity data is a fit to $\sigma_t = \sigma_0 + AC_{oi}^n$ where C_{oi} = number of interstials per formula unit : σ_o = 8.01x10^{-6} Scm^{-1} A=2.2(7) n=2.7(2). This line is presented as a guide to the eye. The post measurement XRD is given in Figure S5a

There is a transition (Figure 8) in the conductivity of the x = 0.54 material, where the T phase is long-range stable at all temperatures, at a similar temperature to that found for the electrical and long-range structural transition in the ambient temperature O phase x = 0.64 material. The activation energy increases from 0.52 eV to 0.98 eV at this point – both activation energies are lower than those found at x = 0.64 which is O at low T. The interstitial carrier ordering which condenses into a long-range structural phase transition to the O phase beyond x = 0.6 thus exercises a clear influence, assigned to short-range order (SRO), on the temperature dependence of the conductivity of compositions which border the onset of the transition, suggesting that the same type of carrier association is happening at this temperature in both x = 0.54 and x = 0.64 materials but that it is short-range only at x = 0.54. Above the T/O structural phase transition, the more highly doped x = 0.64 material is more conducting, whereas below the ordering transition, the x = 0.54 material, which remains T with long-range carrier disorder, is more conducting. This shows the more pronounced effect of the long-range carrier ordering on the ionic transport behavior.

The variation of the conductivity with dopant concentration x is thus complicated by the effect of the long-range ordering into the O phase at high x and the associated impact of SRO in the T phases before the structural phase transition occurs with increasing x. The total conductivity at 800 °C (Figure 10 (b)) of $La_{1+x}Sr_{1-x}Ga_3O_{7+0.5x}$ increases as the activation energy decreases to x = 0.6, which is the stability limit of the T phase at room temperature. For the higher x, O phase materials the activation energy increases and the 800 °C conductivity decreases i.e. the materials which have the carrier ordered O structure at low temperature (x = 0.62 and x = 0.64) have a lower conductivity than x = 0.6 (T structure at low temperature) despite both x = 0.62 and x = 0.64 having more oxygen interstitial charge carriers. Since at 800 °C all the compounds are T, this suggests that short range order persists through carrier-dopant association and reduces the conductivity even in the disordered T phase for the high values of x which produce the ordered phase at low temperature. Thus the highest conductivity is found at the

stability limit of the T phase, despite the higher carrier concentration in the O phase even at O compositions above the temperature of the structural phase transition. Below 565 °C, the maximum conductivity is reached at lower x, for example at 450 °C, x = 0.56 (see SI Figure S6) has the highest conductivity, because the interstitial carrier order associated with the O phase reduces the large x, low temperature conductivity. Thus at all temperatures the highest conductivities are found in materials that do not show the O structural ordering of the carriers. Carrier-dopant association associated with symmetry lowering has been observed in the isolated anion interstitial system $La_{10}(GeO_4)_{6-x}(GaO_4)_xO_{3-x/2}$ where the conductivity decreases above x = 0.125. [19]

The rate of increase in conductivity with x (Figure 10 (b)) decreases as x increases, consistent with carrier ordering or mobility blocking associated with the T/O transition. This contrasts with the linear behavior observed for $Ba_{1-x}La_xIn_2O_{5+x}$ [20] and may be associated with short range order that acts as a precursor to the long range order that causes the T to O transition.

The diffusion coefficient per carrier, D, can be computed from the equation

$$\mathbf{D = \sigma / [(nq^2)/(kT)]}$$

where n is the number of mobile species per cm^3 of material and q the charge of the mobile species. In this case the mobile species are the oxide interstitials. Figure 11 (a) shows D over the 400-950 °C range. At 950 °C the diffusion coefficients are of the order of 10^{-6} to 10^{-5} cm^2s^{-1} (with a maximum of 1.6 x 10^{-5} cm^2s^{-1} at x = 0.6) which compares with conductivity-derived D of 1 x 10^{-6} cm^2s^{-1} for $La_{0.9}Sr_{0.1}Ga_{0.8}Mg_{0.2}O_3$ [21] (validated with tracer diffusion). The diffusion coefficient at 800 ºC (Figure 11 (b)) increases until x = 0.6, with a 13-fold increase from x = 0.1 to the maximum at 0.6. The decrease of conductivity at higher interstitial content (x = 0.62/0.64) correlates with the reduced diffusion coefficient and E_a increase, associated with short-range structural ordering premonitory to the O phase transition and associated blocking of the interstitial mobility. Such long range interactions of carriers have been observed by Hohnke in $Zr(M)O_{2-x}$ $Ce(M)O_{2-x}$ and $Th(M)O_{2-x}$ (M=Sc Y Ca). [22, 23] Vacancy

disordering is also known to produce a threefold increase in conductivity at the fluorite pyrochlore boundary in $Ln_2Zr_2O_7$.[24] In LSGM [13] vacancy carrier trapping premonitory to long-range ordering identified in electron diffraction is proposed to impact the conductivity.

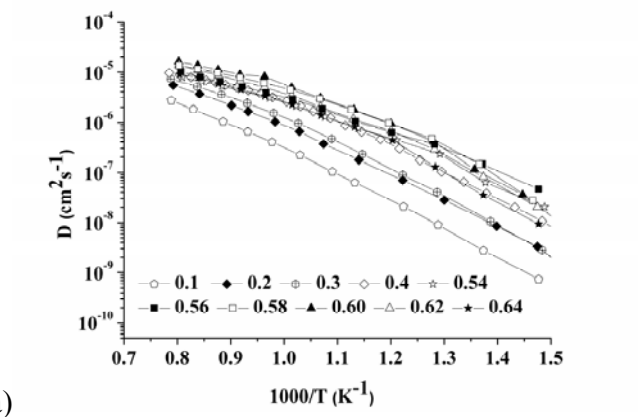

(a)

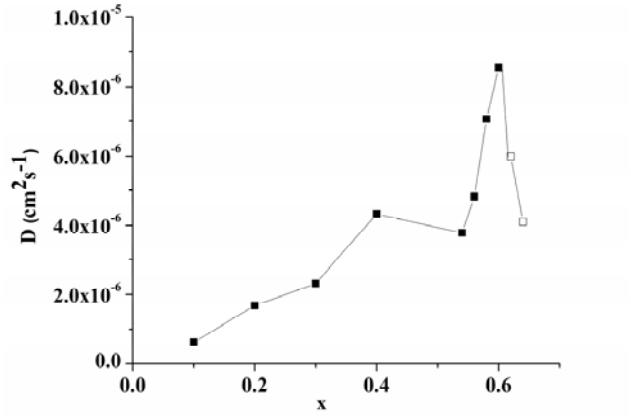

(b)

Figure 11. (a) Diffusion coefficients of $La_{1+x}Sr_{1-x}Ga_3O_{7+x/2}$ (x = 0-0.64) **(b)** Diffusion coefficient versus x at 800 ºC.

Conclusions

The solid solution range in $La_{1+x}Sr_{1-x}Ga_3O_{7+0.5x}$ extends to x = 0.64. The high interstitial oxide content drives a structural phase transition at x > 0.6 from a high temperature tetragonal phase to a low temperature O phase (< 565 °C) which strongly reduces the ionic conductivity, consistent with the transition being produced by static structural order of the interstitial charge carriers. The highest conductivities at any temperature are found in materials where the T structure is stable and interstitial order does not occur, because of the strong influence of short-range ordering associated with the T/O

phase transition at temperatures above the transition, and the associated effect on the temperature and dopant density dependence of the conductivity.

Acknowledgment. We thank EPSRC (EP/C511794/1) and the EU (European Research Council) for support and the STFC for access to Diamond, where we thank Dr. C. Tang, Dr. J .Parker and Dr. S. Thompson for assistance on the I11 diffractometer.

Supporting Information Available: Variable temperature powder X-ray diffraction data, further discussion of the impedance data, Post measurement XRD patterns, Conductivity versus x data at 450°C, Diffuse Reflectance graph and XRDs from annealing experiments. This materials is available free of charge via the Internet at http://pubs.acs.org.

References

(1) K. Eguchi, R. Kikuchi, T. Takeguchi, Elec. Soc. S. **2003**, *2002-2026*, 38-52.

(2) N. Q. Minh, J. Am. Ceram. Soc. **1993**, *76*, 563-588.

(3) D. J. L. Brett, A. Atkinson, N. P. Brandon, S. J. Skinner, Chem. Soc. Rev. **2008**, *37*, 1568-1578.

(4) B. C. H. Steele, Solid State Ionics. **2000**, *129*, 95-110.

(5) A. Lashtabeg, S. J. Skinner, J. Mater. Chem. **2006**, *16*, 3161-3170.

(6) B. C. H. Steele, A. Heinzel, Nature **2001**, *414*, 345-352.

(7) M. Rozumek, P. Majewski, H. Schluckwerder, F. Aldinger, K. Kunstler, G. Tomandl, J. Am. Ceram. Soc. **2004**, *87*, 1795-1798.

(8) M. Rozumek, P. Majewski, L. Sauter, F. Aldinger, J. Am. Ceram. Soc. **2004**, *87*, 662-669.

(9) X. Kuang, M. A. Green, H. Niu, P. Zajdel, C. Dickinson, J. B. Claridge, L. Jantsky, M. J. Rosseinsky, Nat. Mater. **2008**, *7*, 498-504.

(10) M. Steins, W. Schmitz, R. Uecker, J. Doerschel, Z. Krist-New. Cryst. St. **1997**, *212*, 76.

(11) J. R. Macdonald, Impedance Spectroscopy Emphasizing solid materials and systems, Wiley, New York, USA **1987**.

(12) J. R. Macdonald, Ann. Biomed. Eng. **1992**, *20*, 289-305.

(13) K. Q. Huang, R. S. Tichy, J. B. Goodenough, J. Am. Ceram. Soc. **1998**, *81*, 2565-2575.

(14) H. Yoshioka, Chem. Lett. **2004**, *33*, 392-393.

(15) L. Leon-Reina, E. R. Losilla, M. Martinez-Lara, M. C. Martin-Sedeno, S. Bruque, P. Nunez, D. V. Sheptyakov, M. A. G. Aranda, Chem. Mater. **2005**, *17*, 596-600.

(16) G. Dotelli, C. M. Mari, R. Ruffo, R. Pelosato, I. N. Sora, Solid State Ionics**. 2006**, *177*, 1991-1996.

(17) J. B. Goodenough, Ann. Rev. Mater. Res. **2003**, *33*, 91-128.

(18) T. S. Zhang, J. Ma, H. Cheng, S. H. Chan, Mater. Res. Bull. **2006**, *41*, 563-568.

(19) E. Kendrick, P. R. Slater, Mater. Res. Bull. **2008**, *43*, 3627-3632.

(20) K. Kakinuma, H. Yamamura, H. Haneda, T. Atake, Solid State Ionics **2001**, *140*, 301-306.

(21) T. Ishihara, J. A. Kilner, M. Honda, Y. Takita, J. Am. Chem. Soc. **1997**, *119*, 2747-2748.

(22) D. K. Hohnke, J. Phys. Chem. Solids. **1980**, *41*, 777-784.

(23) M. D. Hurley, D. K. Hohnke, J. Phys. Chem. Solids. **1980**, *41*, 1349-1353.

(24) H. Yamamura, H. Nishino, K. Kakinuma, K. Nomura, Solid State Ionics. **2003**, *158*, 359-365.

(25) H. W. Eng, P. W. Barnes, B. M. Auer, P. M. Woodward, J Solid State Chem **2003**, *175*, 94-109.

(26) R. Aleksiyko, M. Berkowski, J. Fink-Finowicki, P. Byszewski, R. Diduszko, E. Kowalska, P. Soc. Photo-Opt. Ins. **2001**, *4412*, 50-54.

(27) J. Ahman, G. Svensson, J. Albertsson, Acta Crystallogr. C. **1996**, *52*, 1336-1338.

(28) S. Li, F. Schonberger, P. Slater, Chemical Communications **2003**, 2694.

(29) F. Schonberger, E. Kendrick, M. S. Islam, P. R. Slater, Solid State Ionics **2005**, *176*, 2951.

(30) K. H. Lee, J. H. Kim, H. L. Kim, S. Kim, H. L. Lee, Japanese Journal of Applied Physics **2005**, *44*, 254.

(31) F. Giannici, D. Messana, A. Longo, L. Sciortino, A. Martorana, Journal of Physics: Conference Series **2009,** *190, 012077*

Chris I. Thomas, Xiaojun Kuang, Zengqiang Deng, Hongjun Niu, John B. Claridge *and* Matthew J. Rosseinsky

Chem. Mater.

Interstitial oxide ion conductivity in the two-dimensional network melilite structure decreases at a structural ordering transition at high ($x > 0.6$) doping levels, with short-range ordering effects influencing the temperature- and composition-dependence of the conductivity even in materials not showing long-range order.